Monatsh Chem (2010) 141:7–13
DOI 10.1007/s00706-009-0229-0

ORIGINAL PAPER

Rapid solidification of cryolite and cryolite–alumina melts

Marián Kucharík · Michal Korenko · Dušan Janičkovič · Magdaléna Kadlečíková · Miroslav Boča · Jozef Vincenc Oboňa

Received: 21 May 2009 / Accepted: 22 November 2009 / Published online: 15 December 2009

Abstract Rapid solidification processing (with a cooling rate in the interval 10^5–10^6 K s^{-1}) was used to prepare deeply undercooled cryolite–alumina melts. These samples were analyzed by XRD, infrared, and Raman spectroscopy. Besides cryolite, the amorphous phase and a low amount of ι-Al_2O_3 were detected. Annealing of the quenched sample revealed the transformation of metastable amorphous phases into different products depending on the annealing conditions. The results obtained showed that all of the elements (Na, Al, O, and F) are probably present in the amorphous parts of the quenched samples.

Keywords Hall–Héroult process · Oxofluoroaluminates · α-Al_2O_3 · β-Al_2O_3 · ι-Al_2O_3

M. Kucharík (✉) · M. Korenko · M. Boča
Institute of Inorganic Chemistry, Slovak Academy of Sciences, Dúbravská cesta 9, 845 36 Bratislava, Slovakia
e-mail: Marian.Kucharik@savba.sk; uachkuch@savba.sk

D. Janičkovič
Institute of Physics, Slovak Academy of Sciences, Dúbravská cesta 9, 845 36 Bratislava, Slovakia

M. Kadlečíková
Department of Microelectronics, Faculty of Electrical Engineering and Information Technology, Slovak University of Technology, Ilkovičová 3, 812 19 Bratislava, Slovakia

J. V. Oboňa
Institute of Electrical Engineering, Slovak Academy of Sciences, Dúbravská cesta 9, 841 04 Bratislava, Slovakia

Introduction

Cryolite (Na_3AlF_6) and alumina (Al_2O_3) are the main constituents of the electrolyte used for industrial production of aluminum in the Hall–Héroult process. Knowledge of the structural features of the various entities formed versus the composition of the cryolite–alumina melt may be of great importance when interpreting physicochemical and electrochemical properties.

Numerous suggestions have been reported regarding the nature of the supposed oxygen-containing species in the melt over the last 70 years of investigations into cryolite–alumina melts. An attempt at a historical overview was made [1], together with a critical discussion. The molten cryolite–alumina system is a mixture with a complex composition. Different ionic entities are assumed to be present, ranging from the simplest sodium cations to larger fluoroaluminate and oxofluoroaluminate anions. However, the reported structural motifs of the complex anions are still controversial [2].

The presence of oxofluoroaluminate species was demonstrated spectrally in the fused salts [3–5]. However, it is unclear whether they exist in the solidified system. Only Brooker et al. [6] have assigned bands to the $Al_2OF_6^{2-}$ anion in the solid state based on Raman and IR spectra of a premelted solid sample containing 5 mol% Na_2O and 5 mol% AlF_3 in FLiNaK (eutectic mixture of LiF–NaF–KF). Na_2O was used as a source of oxygen, as alumina is almost insoluble in FLiNaK.

Nowadays, it is generally accepted that $Al_2OF_6^{2-}$ and $Al_2O_2F_4^{2-}$ are the most probable oxygen-containing ionic entities present at low alumina or high alumina concentrations, respectively. The presence of some other oxygen-containing complex ions in the considered system is still an open question [2].

In the present work, so-called rapid solidification processing (RSP) was applied to prepare deeply undercooled samples of cryolite–alumina molten systems. RSP is used in different fields of material engineering to prepare special amorphous materials (glassy metals, etc.) with interesting properties. This quenching technique permits the solidification of samples at a cooling rate of 10^5–10^6 K s^{-1}, and it has only rarely been used in investigations of molten chemistry (except in glass chemistry) up to now. Using such a cooling rate, we tried to approach in situ high-temperature state conditions (i.e., deeply undercooled melts). Samples prepared in this way were analyzed by means of X-ray powder diffraction (XRD), infrared (IR) and Raman spectroscopy, and energy dispersion X-ray spectroscopy (EDX).

Results and discussion

The products of rapid quenching are shown in Fig. 1. The sample marked as A, which has different transparent needle-like shapes, is the quenched pure molten cryolite. The needle-shaped particles with different widths and lengths denoted B, C, and D are quenched molten mixtures of Na_3AlF_6–Al_2O_3 with 10 wt% (B), 20 wt% (C), and 30 wt% (D) of alumina (in the subsequent text we will denote corundum as "α-Al_2O_3" and use the term "alumina" when discussing Al_2O_3 in general). Each needle sometimes had a central area that was transparent and glass-like, opaque, polycrystalline edges, or vice versa. All of the needle-shaped particles were very brittle. The randomly shaped aggregates with different sizes denoted E, F, and G are quenched molten mixtures of Na_3AlF_6–Al_2O_3 with 10 wt% (E), 20 wt% (F), and 30 wt% (G) of alumina. All of the aggregates were hard and compact.

The shapes of the quenched products were most probably considerably influenced by the variations in the viscosity of the melt due to various alumina contents in the system. The viscosity of the Na_3AlF_6–Al_2O_3 molten system sharply increases with increasing alumina content [7].

The background-subtracted XRD patterns of the quenched samples are shown in Fig. 2. Note that some characteristic features of the amorphous phase (see below) in the measured patterns can be masked by the background caused by scattering in air, and so cannot be analyzed in this experimental arrangement.

The XRD pattern of pure cryolite (sample A) showed only diffractions of the α-Na_3AlF_6 phase. High-intensity diffractions of α-Al_2O_3 were observed in XRD patterns of samples D and G, and one slight diffraction of α-Al_2O_3 was observed in sample C too. However, no diffractions of α-Al_2O_3 were observed in the samples B, E, and F with lower alumina contents. It is evident that, despite using a

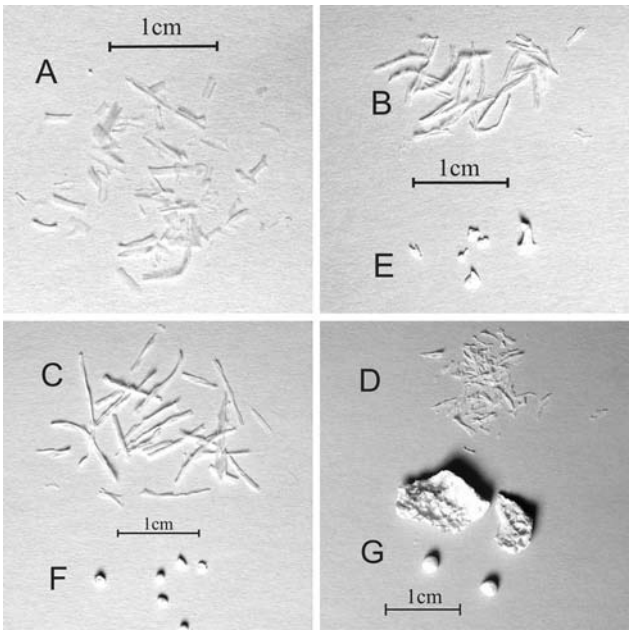

Fig. 1 Photos of the products of rapid quenching: *A*, cryolite; *B*, *E*, cryolite with 10 wt% of alumina; *C*, *F*, cryolite with 20 wt% of alumina; *D*, *G*, cryolite with 30 wt% of alumina

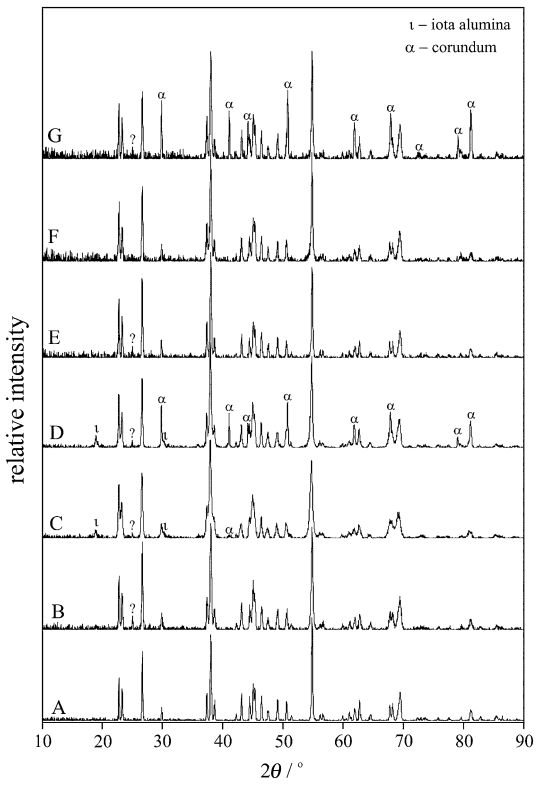

Fig. 2 X-ray powder diffraction patterns of the samples: *A*, quenched cryolite; *B*, *E*, quenched mixture of 90 wt% cryolite and 10 wt% alumina; *C*, *F*, quenched mixture of 80 wt% cryolite and 20 wt% alumina; *D*, *G*, quenched mixture of 70 wt% cryolite and 30 wt% alumina; *B*, *C*, and *D*, needles; *E*, *F*, *G*, aggregates

higher temperature, above the primary crystallization temperature of the mixture melt outflows from the graphite crucible before complete dissolution of the alumina occurred. This cannot be overcome, as the melt starts to outflow from the crucible immediately upon melting. Optimizing the quenching procedure did not help significantly (changing the quenching temperature, heating time, pressure of inert gas above the sample). Employing a higher quenching temperature and increasing the heating time caused evaporation and changes in mixture composition. The presence of undissolved alumina in the molten cryolite probably caused the formation of solid and hard aggregates.

Two slight but intense diffractions at $2\theta = 18.9°$ and $2\theta = 30.0°$ were recorded in the XRD patterns of samples C and D, labeled ι (iota) in Fig. 2. A similar observation was made by Foster [8, 9]. The extracted alumina phase from the quenched mixture had an XRD pattern that was similar to mullite ($3Al_2O_3{\cdot}SiO_2$) [8, 9], so he called it "m-Al_2O_3." This m-Al_2O_3 exhibits the most intense diffractions at ca. $2\theta = 19°$ and $2\theta = 30°$ (ICDD card no. 12-539, denoted iota, ι-Al_2O_3, too these days). It is interesting that so-called mullite-type sodium aluminate prepared by other procedures [10–13] exhibits nearly, if not exactly, identical XRD patterns to the m-Al_2O_3 first reported by Foster [8, 9].

Weak diffraction at $2\theta = 25.0°$ (labeled with a question mark, "?") was observed in all XRD patterns except for samples A and F. This diffraction is not characteristic of any known compound containing the elements Na, Al, O, and F. It should be noted that β-SiO_2, cristobalite (ICDD card no. 27-605), and also $Na(AlSiO_4)$ (ICDD card no. 81-2081) show their most intense diffractions at exactly this position. However, the EDX analysis of the reactants, all of the quenched products, and the graphite crucible showed only very low contents of silicon (Si was detected in only one case among 20 test points, and was below 0.15 wt%). This means that the introduction of silicon from the starting compounds, the graphite crucible, and the quartz tube can be excluded. On the other hand, the EDX analysis showed the presence of a large amount of carbon (1–6 wt%) arising from the graphite crucible. The XRD record for the powdered graphite crucible excluded the idea that the weak diffraction at $2\theta = 25.0$ belonged to the pure carbon phase.

Concerning the IR spectra, continuous growth in the intensity of the broad peak centered at 870 cm^{-1} with increasing alumina content is obvious in all samples (Fig. 3). Simultaneously, an increase in the intensity of the shoulder at 502 cm^{-1} is visible in the IR spectra of samples B, C, D, and G. Both of these broad peaks probably belong to the amorphous parts of the quenched samples (not detectable by XRD). The peak centered at 870 cm^{-1} is in the region of AlO_4 tetrahedra, and the peak centered at

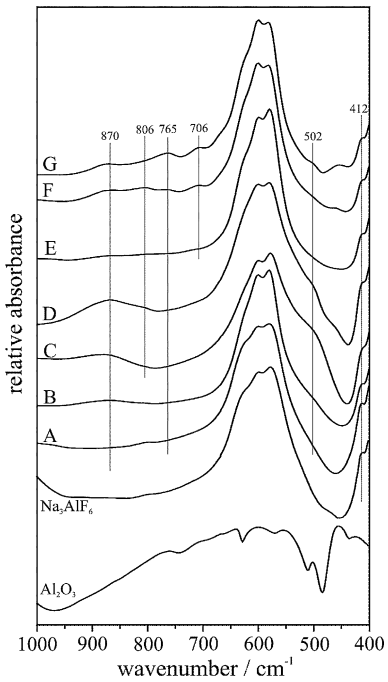

Fig. 3 Infrared spectra of the samples: *A*, quenched cryolite; *B*, *E*, quenched mixture of 90 wt% cryolite and 10 wt% alumina; *C*, *F*, quenched mixture of 80 wt% cryolite and 20 wt% alumina; *D*, *G*, quenched mixture of 70 wt% cryolite and 30 wt% alumina; *B*, *C*, *D*, needles; *E*, *F*, *G*, aggregates

502 cm^{-1} that overlaps with the relatively narrow vibrations of α-Al_2O_3 is in the region of AlO_6 octahedra. Therefore, it can be assumed that aluminum atoms exhibit both tetrahedral and octahedral coordination in the amorphous parts of the quenched samples.

The increases in the intensities of the peaks at 600 cm^{-1} and at $\sim$460 cm^{-1} are associated with the presence of undissolved alumina (samples D, F, and G, Fig. 4). This observation is supported by XRD patterns of samples D and G. The IR spectrum of sample F reveals the presence of α-Al_2O_3, in contrast to XRD, as IR is much more sensitive. Another peak belonging to α-Al_2O_3 was observed in samples F and G ($\sim$765 cm^{-1}). An unassigned peak at 706 cm^{-1} can be identified in samples D, E, F, and G, and another one at 806 cm^{-1} in samples D and F.

Brooker et al. [6] observed Raman and IR spectra, with bands being assigned to the oxofluoroaluminate anion $Al_2OF_6^{2-}$ in the solid state at 25 °C. Brooker's IR spectrum showed relatively broad peaks with maxima at 890, 809, 785, 675, and 640 cm^{-1}. The positions of the first two peaks correspond approximately to the positions of the peaks recorded in the IR spectra of all of the quenched samples (Fig. 3). The last two peaks were not observed, as they can overlap with strong vibrations of cryolite. Based on Brooker's results, it can be suggested that the vibrations in the range 800–600 cm^{-1} belong to the phase that was presented by Brooker as oxofluoroaluminates.

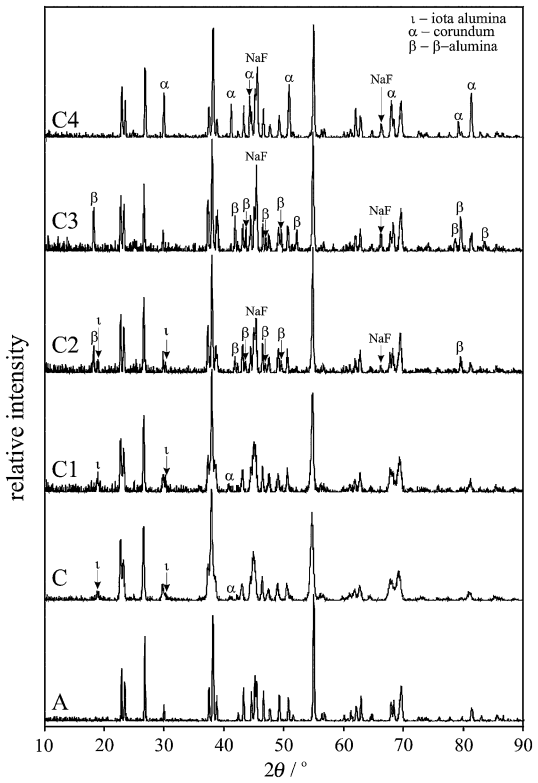

Fig. 4 X-ray powder diffraction patterns of the samples: *A*, quenched pure cryolite; *C*, quenched mixture of 80 wt% cryolite and 20 wt% alumina; *C1*, sample C annealed at 550 °C for 1 h, air atmosphere; *C2*, sample C annealed at 750 °C for 1 h, air atmosphere; *C3*, sample C annealed at 950 °C for 1 h, air atmosphere; *C4*, sample C annealed at 950 °C for 1 h, inert (N_2) atmosphere

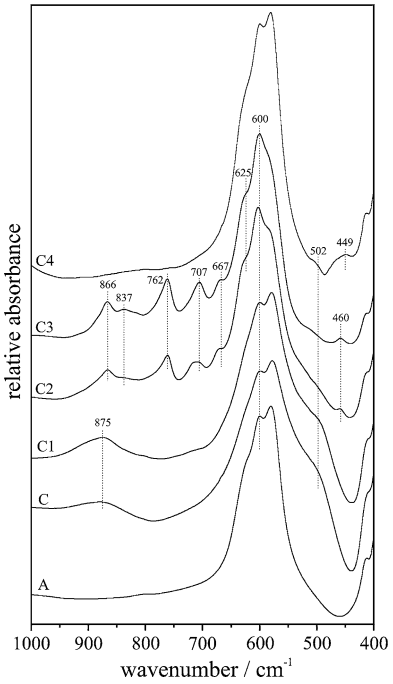

Fig. 5 IR spectra of the samples: *A*, quenched pure cryolite; *C*, quenched mixture of 80 wt% cryolite and 20 wt% alumina; *C1*, sample C annealed at 550 °C for 1 h, air atmosphere; *C2*, sample C annealed at 750 °C for 1 h, air atmosphere; *C3*, sample C annealed at 950 °C for 1 h, air atmosphere; *C4*, sample C annealed at 950 °C for 1 h, inert (N_2) atmosphere

However, they used a very low concentration of the oxygen-containing compound (Na_2O), producing predominantly the $Al_2OF_6^{2-}$ anion in the molten state and the respective compound $Na_2Al_2OF_6$ in the solid state. On the other hand, a considerably higher concentration of alumina in cryolite was used in the present work. Therefore, the presence of the oxofluoroaluminate anion $Al_2O_2F_4^{2-}$ in the liquid state or the respective compound $Na_2Al_2O_2F_4$ (NaAlOF$_2$ [1]) in the solid state can be discussed based on the literature data [1, 2, 14–16].

Peaks assigned only to cryolite were recorded in the Raman spectra of samples A, B, and C. No shifts in peak position were observed, only a decrease in the intensities of cryolite vibrations is observed with increasing amounts of alumina. Similar behavior was observed by Brooker et al. [6]. They supposed that the added α-Al_2O_3 probably converted into γ-Al_2O_3 (gamma alumina) or η-Al_2O_3 (eta alumina) [6]. Neither of these forms of alumina exhibit any bands in the Raman spectrum [17]. In the Raman spectrum of sample D, a fluorescent background with a weak peak at 550 cm^{-1} was observed, which can be assigned to cryolite. In the Raman spectra of samples E and F, no bands were observed except for a weak peak from cryolite in sample E. A very broad band with its maximum at 640 cm^{-1} belonging to α-Al_2O_3 and a very weak peak from cryolite were recorded in the Raman spectrum of sample G (see XRD and IR, Figs. 2, 3).

In order to determine the temperature stability of the amorphous phase, we annealed sample C at different temperatures and conditions (C1–C3: in air; C4: under an inert atmosphere). Some preliminary results have already been published by Korenko et al. [18].

Figure 4 shows the influence of the annealing process on the XRD patterns of the rapidly quenched cryolite–alumina sample C. No differences were observed between the XRD patterns of the samples C and C1 (tempered at 550 °C in air). The XRD patterns of samples C2 (750 °C, air) and C3 (950 °C, air) revealed the presence of NaF, β-alumina ($NaAl_{11}O_{17}$), and cryolite. The diffractions of ι-Al_2O_3 and those of undissolved primary α-Al_2O_3 were not seen for sample C3, in contrast with the original sample C. Sample C annealed under an inert (N_2) atmosphere (C4, at 950 °C) contains NaF, α-Al_2O_3, and cryolite.

No differences between the IR spectra of samples C and C1 were observed (Fig. 5). The broad band centered at ~870 cm^{-1} starts to show fine structure in samples C2 and C3, which means an increase in the quality of crystallinity.

An increase in the content of the crystalline phase is also supported by a narrowing of the shoulder at ~ 502 cm^{-1} from C1 to C3. Although the XRD patterns of samples C2 and C3 revealed the presence of β-alumina, we are not aware of any relevant IR record for this compound. Generally, Al–O vibrations for different types of sodium aluminates are reported to occur in the region 1,000–450 cm^{-1} [19, 20]. The IR spectrum of sample C4 only showed peaks belonging to cryolite and α-Al_2O_3 (Fig. 5), in accordance with XRD analysis (Fig. 4).

The Raman spectrum of the annealed sample C3 showed a fluorescent background with a small peak at 550 cm^{-1}, assigned to cryolite. It follows that some of the compounds causing the fluorescent background must have been formed during annealing in air. Alumina occurs in several known phases, but there are only two forms, γ-Al_2O_3 and η-Al_2O_3, that produce fluorescent background in Raman spectra. Therefore, the presence of either form of alumina could be assumed, even though they have not been confirmed by XRD (in Raman spectra, levels of ppm can cause such fluorescent effects). A similar fluorescent background was observed in the Raman spectrum of the quenched sample D.

Based on the above results it is evident that the formation of β-alumina or α-Al_2O_3 is influenced by the presence of air or an inert atmosphere, respectively.

The formation of β-alumina was also recorded in our previous work [21]. The XRD patterns of long-term annealed (50 h) mixtures of the system Na_3AlF_6–Al_2O_3 (30 mol% alumina) under an air atmosphere and in the region of the coexistence of liquid and solid phases (the working temperature was 1,010 °C) showed the presence of β-alumina, α-Al_2O_3, NaF, and cryolite. We suppose that β-alumina is a product of the reaction between NaF and α-Al_2O_3 according to the following reaction [22]:

$$2\mathrm{NaF(l)} + (3x+1)/3\mathrm{Al_2O_3(s,\ alpha)} \rightarrow \mathrm{Na_2O \cdot} x\mathrm{Al_2O_3(s)} + 2/3\mathrm{AlF_3(l)} \quad (1)$$

NaF, a reactant in the above reaction, was produced by the evaporation of $NaAlF_4$ from cryolite according to the following known reaction [23]:

$$\mathrm{Na_3AlF_6} \rightarrow 2\mathrm{NaF} + \mathrm{NaAlF_4(g)} \quad (2)$$

However, this reaction occurs at higher temperatures than the annealing temperatures used in this work. Moreover, weight loss analysis before and after annealing suggests that the occurrence of NaF in the samples is not caused by this reaction. An additional annealing test was performed with pure cryolite (using the same amount and the same conditions as used for sample C4) in order to determine the influence of the annealing on the formation/evaporation of $NaAlF_4$. No NaF diffractions were observed in the XRD pattern.

It must be pointed out that the annealing temperature, 950 °C, is still below the eutectic temperature (t_{EUT} = 966 °C) of the binary system Na_3AlF_6–Al_2O_3 [2]. Consequently, the system studied should be in the solid state while annealing at 950 °C. However, an increase in the NaF concentration in the system (i.e., the formation of NaF during annealing) occurs. The temperature of the located ternary eutectic point in the ternary system Na_3AlF_6–NaF–Al_2O_3 (CR $\geq$ 3, CR = n(NaF)/n(AlF_3)) is approximately 880 °C [24]. This indicates that the liquid and the solid phase could coexist in the system while annealing at 950 °C. This was also confirmed by visually checking the sample after the annealing. The surface of the sample was evidently pre-melted. On the other hand, sample C2, which was heated to only 750 °C, had to be in a solid state during the annealing (there were also no visually observed changes in the sample). Therefore, it can be concluded that the NaF detected is a product of the decomposition of the amorphous part of sample C in both cases of annealing (air or inert atmosphere).

A similar observation was made by Bache and Ystenes [25]. They quenched molten equimolar mixtures of chiolite ($Na_5Al_3F_{14}$) and cryolite with 10% of alumina by pouring the melt directly into water (0 °C). Transformation of the quenched samples during annealing should liberate fluorides, and hence slightly increase the chiolite/cryolite ratio.

Regarding the formation of β-alumina (samples C2 and C3) or α-Al_2O_3 (C4) in terms of the phase diagram of the system Na_3AlF_6–NaF–Al_2O_3, β-alumina is precipitated as a primary phase at higher contents of NaF and alumina. This indicates that the system for sample C4 did not pass across the univariant line between β-alumina and α-Al_2O_3 during annealing, in contrast to samples C2 and C3.

In the case of pure amorphous alumina, the transition to γ-Al_2O_3 and then to α-Al_2O_3 upon heating has been observed by different authors [26–28].

Based on the above results, it is evident that the formation of β-alumina is influenced by the presence of air. Nevertheless, the difference between the annealing products β-alumina (air atmosphere) and α-Al_2O_3 (inert atmosphere) can be explained by the slight liberation of $NaAlF_4$ vapor in sufficient amounts upon passing from the crystallization region of α-Al_2O_3 to the crystallization region of β-alumina. The second and more reliable explanation could be that the amorphous form reacted with oxygen and the traces of humidity introduced into the system from the air produced more stable β-alumina and NaF (HF should be released). In the inert atmosphere, only the conversion of amorphous (metastable) phases to more stable α-Al_2O_3 and NaF occurred. Finally, it could be supposed that all of the elements (Na, Al, O, F) are present in the amorphous metastable phase of sample C.

Conclusion

The aim of this work was to analyze the samples prepared by RSP. The primary intention was to obtain a metastable phase that has structural features that exist in the liquid phase of the cryolite–alumina system.

Samples prepared by RSP contained a certain amount of amorphous phase. In some cases, a small amount of crystalline ι-Al_2O_3 was detected by XRD. Annealing of the quenched sample C (20 wt% alumina) revealed the transformation of metastable amorphous phases into different products depending on the annealing conditions. When an air atmosphere was placed in contact with the annealed sample C, the formation of β-alumina and NaF was observed as result of the reaction with oxygen from the humidity in the air. On the other hand, insufficient oxygen and trace water (inert atmosphere, N_2) resulted in the formation of the most stable α-Al_2O_3. These results showed that all of the elements (Na, Al, O, and F) are present in the amorphous parts of the quenched samples, and so we can agree with the tentative conclusion of Foster [8], that amorphous oxofluoroaluminate compounds that are probably captured by rapid quenching and are also in the liquid phase could have a skeletal arrangement similar to that in m-Al_2O_3 (ι-Al_2O_3)—probably having a mullite-type Na-aluminate structure. An additional contribution to resolving the decomposition of the amorphous phases in the quenched samples could be provided by performing in situ high-temperature synchrotron powder measurements or magic angle spinning nuclear magnetic resonance (MAS NMR) spectroscopy. The results from both techniques are currently being evaluated.

Experimental

Equipment

The RSP apparatus consists of an inductive furnace and a rotating cooling Cu wheel (Fig. 6). The thoroughly mixed samples (cryolite–alumina 10, 20, and 30 wt%) were placed in a graphite crucible glued into a quartz tube. At the bottom of the crucible there was a small orifice for melt outflow. The distance between the orifice and the rotating cylinder was approximately 0.2 mm. The quartz housing tube with the crucible and the sample was filled with an Ar atmosphere. This apparatus arrangement permits the solidification of melts from the molten state (in our case around 100 °C above the melting point) to the solid state at room temperature at a cooling rate of about 10^5–10^6 K s^{-1}. Further details of this technique can be found elsewhere [29].

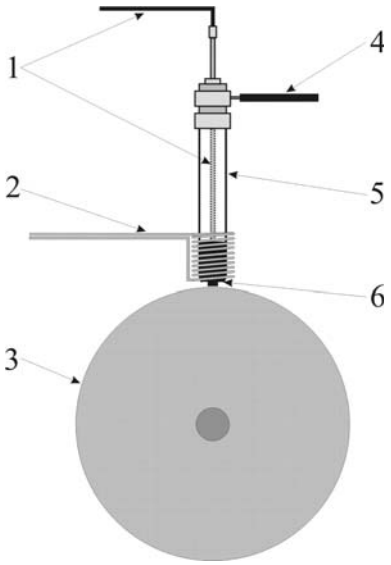

Fig. 6 Apparatus used for the rapid solidification process. *1*, Thermocouple; *2*, inductive furnace; *3*, rotating cooling Cu wheel; *4*, inlet for inert gas (Ar); *5*, quartz tube; *6*, graphite crucible

The quenched sample with 20 wt% of alumina was placed in a platinum crucible and annealed at different temperatures; however, as the experiments were done in the closed furnace without any possibility of looking inside during the experiment, the formation of liquid was not checked for. The process was done in a Kanthal resistance furnace equipped with a vertical alumina tube and calibrated Pt–Pt10Rh thermocouple located close to the platinum crucible.

X-ray diffraction (XRD) patterns were collected at room temperature within the interval 10–90° in steps of 0.02° 2θ using Co $K_{\alpha 1}$ radiation. The samples were mounted on foil. To collect the XRD patterns, a transmission Stoe Stadi P diffractometer equipped with a linear PSD and a curved Ge(1 1 1) primary beam monochromator were used.

The infrared (IR) spectra were obtained using a Nicolet Magna 750 FTIR spectrometer equipped with a DTGS detector. The samples were analyzed in KBr pellets.

The Raman spectra were measured by a Dilor-Jobin–Yvon-Spex Raman spectrometer, type LabRam, with a He–Ne laser excitation source (632.8 nm, 15 mW). Calibration of the spectrometer was performed with respect to the 520.7 cm^{-1} band of single-crystalline silicon.

Elemental analyses were examined by a scanning electron microscope (model EVO 40HV, Carl Zeiss SMT AG, Germany) equipped with a Bruker AXS XFlash 4010 detector (for energy dispersion X-ray spectroscopy, EDX).

Chemicals

Hand-picked powdered cryolite from Greenland, Na_3AlF_6 (melting point: 1,009–1,011 °C), and Al_2O_3 powder

(Merck, p.a.). Both chemicals were dried for several hours at 500 °C before use. Argon gas (Messer, 99.996%).

Acknowledgments Slovak Grant Agencies VEGA 2/7077/27, VEGA 2/0058/09, and APVV-0413-06 are acknowledged for financial support. This publication is the result of the project implementation: Centre for Materials, Layers, and Systems for Applications and Chemical Processes Under Extreme Conditions, supported by the Research & Development Operational Programme, funded by the ERDF.

References

1. Boča M, Kucharík M (2007) Chem Pap 61:217
2. Thonstad J, Fellner P, Haarberg GM, Híveš J, Kvande H, Sterten Å (2001) Aluminium electrolysis, fundamentals of the Hall–Héroult process, 3rd edn. Aluminium-Verlag, Düsseldorf
3. Gilbert B, Mamantov G, Begun GM (1976) Inorg Nucl Chem Lett 12:415
4. Robert E, Olsen JE, Daněk V, Tixhon E, Østvold T, Gilbert B (1997) J Phys Chem B101:9447
5. Lacassagne V, Bessada C, Florian P, Bouvet S, Ollivier B, Coutures JP, Massiot D (2002) J Phys Chem B106:1862
6. Brooker MH, Berg RW, von Barner JH, Bjerrum NJ (2000) Inorg Chem 39:4725
7. Tørklep K, Øye HA (1979) Light metals 1979. In: Proc Sessions of 108th AIME Annual Meeting, New Orleans, LA, 19–21 Feb 1979, p 373
8. Foster PA (1959) J Electrochem Soc 106:971
9. Foster PA (1960) J Am Ceram Soc 43:66
10. Perrotta J, Young JE Jr (1974) J Am Ceram Soc 57:405
11. Elliot G, Huggins RA (1975) J Am Ceram Soc 58:497
12. Mazza D, Vallino M, Busca G (1992) J Am Ceram Soc 75:1929
13. Fischer RX, Schmücker M, Angerer P, Schneider H (2001) Am Mineral 86:1513
14. Førland T, Ratkje SK (1973) Acta Chem Scand 27:1883
15. Sterten Å (1980) Electrochim Acta 25:1673
16. Kvande H (1980) Electrochim Acta 25:273
17. Kadlečíková M, Breza J, Veselý M (2001) Microelectron J 32:955
18. Korenko M, Kucharík M, Janičkovič D (2007) Chem Pap 62:219
19. Jayaraman V, Gnanasekaran T, Periaswami G (1997) Mater Lett 30:157
20. Sartori S, Martucci A, Muffato A, Guglielmi M (2004) J Eur Ceram Soc 24:911
21. Kucharík M, Boca M, Bessada C, Fuess H (2005) Eur J Inorg Chem 9:1781
22. Sterten Å, Hamberg K, Mæland I (1982) Acta Chem Scand 36:329
23. Bruno M, Herstad O, Holm JL (1998) Acta Chem Scand 52:1399
24. Foster PA (1964) J Chem Eng Data 9:200
25. Bache Ø, Ystenes M (1989) Acta Chem Scand 43:97
26. Yu N, McIntire PC, Nastasi M, Sickafus KE (1995) Phys Rev B 8:17518
27. Shek CH, Lai JKL, Gu TS, Lin GM (1997) Nanostruct Mater 8:605
28. Wang Y, Bhandari S, Motra A, Parkin S, Moore J, Atwood DA (2005) Z Anorg Allg Chem 631:2937
29. Jacobson LA, McKittrick J (1994) Mater Sci Eng R 11:355